Acoustics 2008
Geelong, Victoria, Australia 24 to 26 November 2008

Acoustics and Sustainability:

How should acoustics adapt to meet future demands?

Scanning laser vibrometer for non-contact three-dimensional displacement and strain measurements

Ben Cazzolato (1), Stuart Wildy (1), John Codrington (1), Andrei Kotousov (1) and Matthias Schuessler (2)

(1) School of Mechanical Engineering, University of Adelaide, SA, Australia
(2) Polytec GmbH, Polytec-Platz 1-7, 76337 Waldbronn, Germany

ABSTRACT

The recent advent of three-dimensional scanning laser vibrometers has enabled extremely accurate non-contact measurement of the three-dimensional displacements of structures. This paper looks at the feasibility of using a scanning laser vibrometer for the non-contact measurement of dynamic strain fields across the surface of a planar structure. Issues such as laser head alignment and choice of finite-difference scheme are discussed. Finally, experimental results of a test specimen are presented which clearly demonstrate the significant potential of this new experimental technique.

INTRODUCTION

The measurement of displacement, strain and stress fields is important in many fields of applied mechanics and engineering. Such measurements are most commonly conducted by contact techniques using strain gauges, brittle surfaces or piezo-electric sensors, or non-contact methods such as photo-elasticity (Asundi, 1996), x-ray diffraction (Gilfrich 1998) and holographic interferometry (Colchero et al. 2002).

Recent improvements in laser measurement systems have stimulated the application of scanning laser vibrometers to measure the out-of-plane displacement in plate- or shell-like structures, from which the curvature, bending strain and stresses may be estimated via a double spatial derivative (Miles et al. 1994, Moccio et al. 1996, Xu et al. 1996). It should be noted that all previous publications involving the application of laser vibrometers to measure kinematic variables have been restricted to single laser Doppler vibrometry able to measure only bending deformations. Due to poor transducer quality, early applications of the laser vibrometer technique required extensive spatial filtering to improve the quality of the strain estimates, at the expense of spatial resolution.

Recently 3D laser vibrometers have entered the market, which allow the non-contact (remote) measurement of not only the out-of-plane displacement component, but also the in-plane displacement components. Polytec produce a scanning variant of the 3D laser vibrometer as shown in Figure 1.

In an insightful paper on the application on 3D laser vibrometry, Mitchell at al. (1998) suggested that "with the full-surface response descriptions one can consider the development of strain distributions over the surface". It took almost an entire decade before Mitchell's vision became a reality in which 3D laser vibrometry was demonstrated to estimate strain (Schuessler 2007). The three laser heads directly measure velocities in three dimensions at a point, from which displacements and thus strain and stress fields may be evaluated, as opposed to using a single laser head which only enables bending strain to be determined. According to the manufacturer of the PSV-3D, three-dimensional measurement of dynamic surface strain has only been possible in the last few years with the availability of 3D scanning laser vibrometers with sufficient spatial resolution and the associated high resolution decoders.

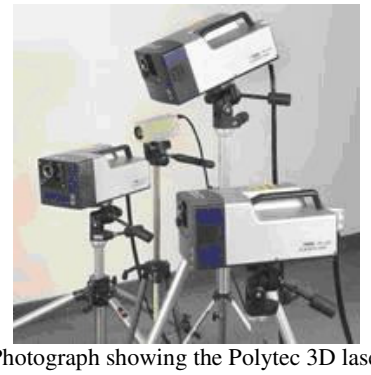

Figure 1. Photograph showing the Polytec 3D laser vibrometer and optional camera. Source Polytec.

In this paper, the application of a Polytec 3D scanning laser vibrometer (PSV-3D) to the measurement of the kinetic variables of a plate structure is presented. The underlying theory of the laser vibrometer and strain theory is initially discussed, followed by an experiment used to test the approach. Advantages and limitations of this technique are also discussed.

STRAIN ESTIMATION VIA DISPLACEMENT MEASUREMENTS

The approach used for estimating the strain from the displacement field obtained from the lasers is the same as that used in Finite Element (FE) modelling. The strain finite element shape functions will now be derived following the technique presented in Fagan (1992). The analysis presented here is for planar structures; however the analysis could be easily extended to three-dimensional structures.

3-noded element

Consider the 3-noded triangular element (shown in Figure 2) with interpolation function $\phi(x,y)=\alpha_1+\alpha_2 x+\alpha_3 y$, where x and y are the coordinates of a point within the element. This function represents how a value (such as the displacement, u or v) varies across the element.

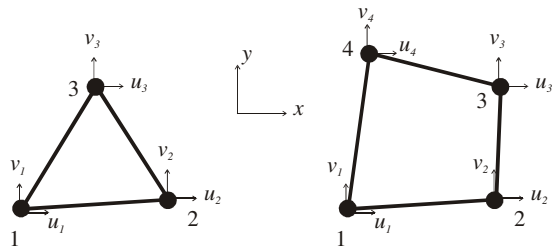

Figure 2. Two-dimensional 3-noded linear and 4-noded bilinear elements.

The real weights α_i are a function of the values of ϕ at each of the three nodes (ϕ_1,ϕ_2,ϕ_3) and are given by

$$\alpha_1 = \tfrac{1}{2A}\left(a_1\phi_1 + a_2\phi_2 + a_3\phi_3\right)$$
$$\alpha_2 = \tfrac{1}{2A}\left(b_1\phi_1 + b_2\phi_2 + b_3\phi_3\right)$$
$$\alpha_3 = \tfrac{1}{2A}\left(c_1\phi_1 + c_2\phi_2 + c_3\phi_3\right)$$

A, the area of the triangular element, is given by

$$A = \tfrac{1}{2}\begin{vmatrix}1 & x_1 & y_1\\ 1 & x_2 & y_2\\ 1 & x_3 & y_3\end{vmatrix} = \tfrac{1}{2}\left(x_1y_2 + x_2y_3 + x_3y_1 - x_1y_3 - x_2y_1 - x_3y_2\right)$$

where

$$a_1 = x_2y_3 - x_3y_2 \quad b_1 = y_2 - y_3 \quad c_1 = x_3 - x_2$$
$$a_2 = x_3y_1 - x_1y_3 \quad b_2 = y_3 - y_1 \quad c_2 = x_1 - x_3$$
$$a_3 = x_1y_2 - x_2y_1 \quad b_3 = y_1 - y_2 \quad c_3 = x_2 - x_1$$

This can be rewritten more compactly in matrix form of the following

$$\phi(x,y) = \mathbf{N}(x,y)\Phi$$

where $\mathbf{N}$ is the FE shape function vector

$\mathbf{N} = \begin{bmatrix}N_1(x,y) & N_2(x,y) & N_3(x,y)\end{bmatrix}$, such that

$N_i(x,y) = \tfrac{1}{2A}\left(a_i + b_i x + c_i y\right)$.

The interpolation function vector is given by

$\Phi = \begin{bmatrix}\phi_1 & \phi_2 & \phi_3\end{bmatrix}^T$, where $[\ ]^T$ is the matrix transpose.

Now consider the displacement $[u,v]^T$ at an arbitrary location $[x,y]^T$. This is given by the product of shape function equations at the location and the vector containing the displacements at the nodes,

$$\begin{bmatrix}u(x,y)\\ v(x,y)\end{bmatrix} = \mathbf{N}(x,y)\mathbf{U}$$

where the shape function matrix is (dropping the spatial dependence $[x,y]^T$) given by

$\mathbf{N} = \begin{bmatrix}N_1 & 0 & N_2 & 0 & N_3 & 0\\ 0 & N_1 & 0 & N_2 & 0 & N_3\end{bmatrix}$ and the column vector of nodal displacements is given by

$$\mathbf{U} = \begin{bmatrix}u_1\\ v_1\\ u_2\\ v_2\\ u_3\\ v_3\end{bmatrix}.$$

Differentiating the displacement vector we can obtain the 2-dimensional strains

$$\varepsilon_x = \frac{\partial u}{\partial x} \quad \varepsilon_y = \frac{\partial v}{\partial y} \quad \gamma_{xy} = \frac{\partial u}{\partial y} + \frac{\partial v}{\partial x}$$

To give the strain-nodal displacement matrix relation:

$$\begin{bmatrix}\varepsilon_x\\ \varepsilon_y\\ \gamma_{xy}\end{bmatrix} = \mathbf{B}\mathbf{U}$$

where **B** is the strain matrix given by

$$\mathbf{B} = \frac{1}{2A}\begin{bmatrix}b_1 & 0 & b_2 & 0 & b_3 & 0\\ 0 & c_1 & 0 & c_2 & 0 & c_3\\ c_1 & b_1 & c_2 & b_2 & c_3 & b_3\end{bmatrix}$$

It should be noted that the strains across linear triangular elements are therefore uniform, and hence it is known as the constant strain element.

4-noded element

A similar approach may be taken to define the strain vector for the 4-noded rectangular bilinear element shown in Figure 2. The formulation presented here is for a rectangular element. For a more general treatment of quadrilateral plate element see Wang et al. (2004) or Kardestuncer (1987).

The displacement field within the element may be interpolated using

$$\begin{bmatrix}u(x,y)\\ v(x,y)\end{bmatrix} = \mathbf{N}(x,y)\mathbf{U}$$

where the displacements at the nodes is given by

$$\mathbf{U} = \begin{bmatrix} u_1 \\ v_1 \\ u_2 \\ v_2 \\ u_3 \\ v_3 \\ u_4 \\ v_4 \end{bmatrix}$$

and the shape function matrix is

$$\mathbf{N} = \begin{bmatrix} N_1 & 0 & N_2 & 0 & N_3 & 0 & N_4 & 0 \\ 0 & N_1 & 0 & N_2 & 0 & N_3 & 0 & N_4 \end{bmatrix}$$ where the individual (bilinear) shape functions as a function of the natural (normalised) coordinates ξ and η are given by

$$N_1 = \tfrac{1}{4}(1-\xi)(1-\eta) \quad N_3 = \tfrac{1}{4}(1+\xi)(1+\eta)$$
$$N_2 = \tfrac{1}{4}(1+\xi)(1-\eta) \quad N_4 = \tfrac{1}{4}(1-\xi)(1+\eta).$$

For rectangular elements the natural (normalised) coordinates are $\xi = \frac{2x - |x_2 + x_1|}{|x_2 - x_1|}$ and $\eta = \frac{2y - |y_2 + y_1|}{|y_2 - y_1|}$.

By spatially differentiating the displacement field, the strain field of a 4-node quadrilateral element is obtained

$$\begin{bmatrix} \varepsilon_x \\ \varepsilon_y \\ \gamma_{xy} \end{bmatrix} = \mathbf{BU}$$

where

$$\mathbf{B}^T = \begin{bmatrix} -\frac{1-\eta}{a} & 0 & -\frac{1-\xi}{b} \\ 0 & -\frac{1-\xi}{b} & -\frac{1-\eta}{a} \\ \frac{1-\eta}{a} & 0 & -\frac{1+\xi}{b} \\ 0 & -\frac{1+\xi}{b} & \frac{1-\eta}{a} \\ \frac{1+\eta}{a} & 0 & \frac{1+\xi}{b} \\ 0 & \frac{1+\xi}{b} & \frac{1+\eta}{a} \\ -\frac{1-\eta}{a} & 0 & \frac{1-\xi}{b} \\ 0 & \frac{1-\xi}{b} & -\frac{1+\eta}{a} \end{bmatrix},$$

$a = \frac{1}{2}|x_2 - x_1| = \frac{1}{2}|x_4 - x_3|$ and $b = \frac{1}{2}|y_4 - y_1| = \frac{1}{2}|y_3 - y_2|$.

POLYTEC PSV-3D SCANNING LASER VIBROMETER

The PSV-3D operates on the Doppler principle and uses three laser heads to measure the instantaneous vibratory displacement in the direction of each laser, from which the displacement components in three orthogonal directions are obtained via an orthogonal decomposition (see Figure 3). The digital velocity decoders used in the PSV are able to measure displacements down to sub-nm range, over a spot size of approximately 40 μm (for Long Range lens) with maximum spatial resolution of approximately 20 μm. The PSV software can measure up to a 512x512 grid. Such a measurement system can theoretically enable unprecedented resolution of dynamic strain measurements down to nanoscale.

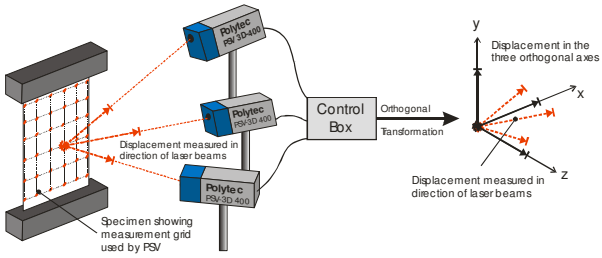

Figure 3. Illustration of experimental arrangement for measurement of the displacement field on a flat plate, from which the strain field can be estimated for the whole surface of the structure.

The angular resolution of the servo mechanisms in the laser heads is <0.002degrees and pointing stability (repeatability) is < 0.01degrees. At a stand off distance of 500mm, this corresponds to 17 μm and 87 μm respectively.

In addition to the three vibrometer lasers the system also has a Geometry Scan Unit which provides approximate measures of the scan points relative to the heads with an accuracy of $\pm$2.5mm. This error is a low wavenumber bias error rather than random error. In other words, the error in displacement measured by the geometry scan unit does not vary randomly, but rather varies slowly with position. Therefore two very closely spaced points do not experience a significant difference in error.

The PSV-3D uses a velocity decoder (VD-07) to resolve the Doppler data to velocity signals. The relevant specifications are: Maximum sensitivity is 1 (mm/s)/V = 1V/(mm/s); Corresponding maximum range is 10 mm/s =10 V; Resolution is 0.02 μm /s/sqrt(Hz); and the lowest frequency is DC.

To measure the kinematic variables (such as strain) it is necessary to undertake the measurements in the frequency domain since the phase information between nodes is essential. Transfer functions between a reference (usually the source of vibration) and the 3 displacements measured by the laser heads provide the necessary phase information. Averaging of the transfer functions screen out non-correlated motion such as air-borne and ground-borne noise. If operating in the stiffness controlled region of the specimen, then additional gains in signal to noise can be achieved by using multiple sinusoids (which are not harmonics of each other) and averaging.

EXPERIMENTS

Experimental Apparatus

To validate the strain measurement system, cyclic tests were undertaken on an as supplied commercial grade aluminium plate (Young's modulus, E = 77GPa). The aluminium was cut into a standard dogbone specimen with the length orientated in the rolling direction (cross-section of 38mm by 12mm and a reduced lengthwise section of 125 mm).

The cyclic tests were carried out on the specimen using an Instron 1342 hydraulic test machine operating under load control. Once the specimen was aligned and clamped into the Instron, the lasers were positioned such that the left laser was below, the top laser was above and the right laser was directly inline with the specimen (as seen in Figure 4). Furthermore, the lasers were placed at an optimal stand-off distance of 711 mm from the specimen to ensure a visibility maximum for the lasers.

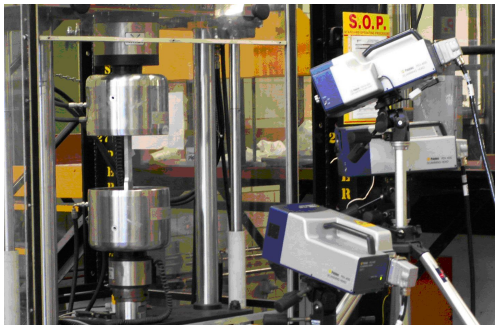

Figure 4. Photograph of the Polytec PSV-3D laser vibrometer focused at an aluminium dogbone specimen clamped in an Instron 1342 hydraulic test machine.

Figure 5 shows a close up of the specimen in the clamps of the Instron as well as the two measurement grids employed; a coarse grid of triangular elements, and a fine grid of rectangular elements. The bright spot in the middle of the grid is the alignment location of the three lasers.

The output from a load cell attached to the Instron was used to provide a reference signal for the laser measurement system.

When aligning the lasers, eleven 2D alignment points (discussed in more detail in the next section) were used and positioned in the general measurement area. The 3D alignment was set up with the x-axis along the breadth and the y-axis in the length of the specimen as shown in Figure 5. In addition, an out of plane 3D alignment point was positioned on the cross-head of the Instron. The accuracy of the 3D alignment was Top laser = 0.0 mm, Left laser = 0.2 mm and Right laser = 0.3 mm. Scan points were then selected in the middle of the specimen, using either a triangular or rectangular grid, as seen in Figure 5.

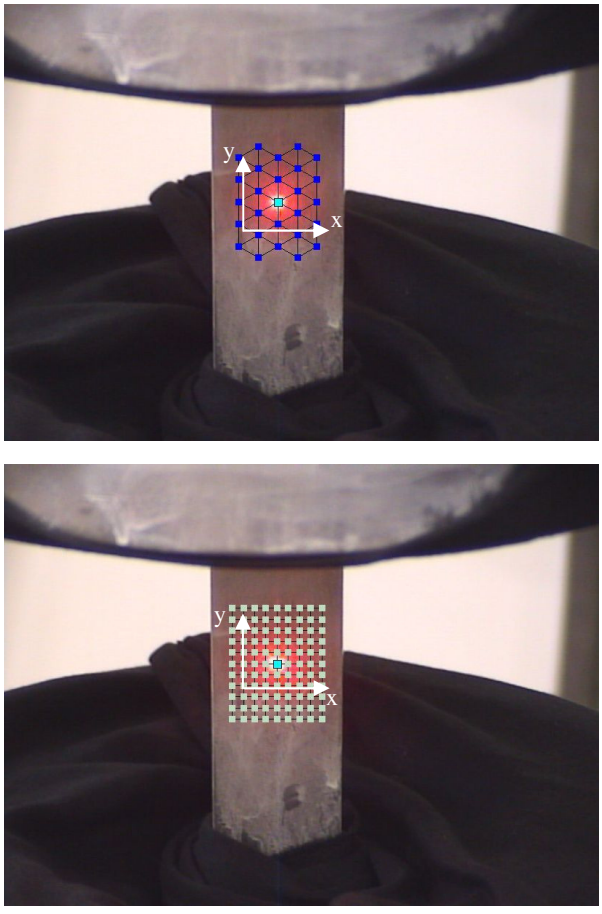

Figure 5. Close up of the aluminium dogbone specimen showing the coarse triangular element measurement grid, the fine rectangular element measurement grid and laser spot.

The analyser was set up such that the vibrometer signal was measured over a 200 Hz bandwidth with a 0.5 Hz frequency resolution and 75% overlap. Complex averaging was employed, using 32 averages, and a flat top window function was utilised to prevent leakage. The coherence between the reference channel (load cell output) and vibration along all three axes exceeded 99.9%.

Displacement Results

During the tests cyclic loading of 19.5kN (peak) was applied to the specimen with a frequency of 5Hz. Since the specimen was driven in its stiffness controlled region, the phase difference between the displacement and the applied force was negligible (less than 1 degree for all measurement points). The scan data including nodal and element geometries, complex nodal displacement spectrum (along x, y and z-axes), reference channel spectrum, frequency response function and coherence were saved as a UFF (universal file format) file. The data was then post-processed in Matlab. The real displacement data for the three orthogonal directions and both measurement grids is presented in Figures 6 to 8.

The peak displacements for the specimens are approximately $[82 \pm 2.5\mu\text{m}, 125 \pm 10\mu\text{m}, 21.5 \pm 0.5\mu\text{m}]$. These displacement figures show that there is both rigid body motion and strain along all three axes despite the specimen being mounted in the Instron which was supposed to induce motion only along the y-axis. The two sets of displacement measurements exhibit the same behaviour indicating that they are either correct or the errors present are systematic rather than stochastic.

Strain Results

The dynamic strain fields in the x-y plane were calculated by applying the previously derived strain interpolation functions to the measured displacements shown in Figures 6 to 8. The mean and standard deviation of the elemental strains for the specimen (in Figures 9 to 11) are

$$[\varepsilon_x, \varepsilon_y, \gamma_{xy}] = [-184 \pm 23\mu\varepsilon, 552 \pm 36\mu\varepsilon, \ 6 \pm 50\mu\varepsilon]$$
$$[\varepsilon_x, \varepsilon_y, \gamma_{xy}] = [-154 \pm 40\mu\varepsilon, 552 \pm 61\mu\varepsilon, \ 4 \pm 69\mu\varepsilon]$$

for the triangular and rectangular grid respectively. The ratio of the x to y strain gives Poisson's ratios of 0.33 and 0.28 respectively.

To provide a comparison to the laser measurements, contact strain measurements were made using a mechanical extensiometer. The extensometer works by measuring the change in displacement between two points on the specimen surface. Flat 'knife edges' contact the specimen at the measurement points and lever arms then transfer the displacement to attached strain gauges. In the present experiments, the gauge length (distance between measurement points) was 50 mm for the y-direction measurements and 25 mm for the x-direction (with a range of +/-0.5 mm). The elongation of the specimen was measured at 10 kN intervals up to 40 kN and logged by a National Instruments 14 bit USB data acquisition device. The normalised results from the extensometer and laser are shown in Table 1. From a regression on this data a Young's modulus of 77.3 GPa and a Poisson's ratio of 0.36 was obtained.

The dynamic x and y strains derived by these two independent methods are as expected and show similar mean values

(see Table 1). The shear strain shows an acceptable mean. The observed variance of the shear strain is too large to be attributed to the grain structure and is a result of systemic errors. If the variances of the x and y displacements are uncorrelated, then one may expect a variance of the shear strain to be approximately twice the variance of the x and y strains, which is what is observed here. The variance of the strains for the fine rectangular grid is greater than for the coarse triangular grid due to the small element size (which is discussed in more detail below).

Table 1. Normalised strains per unit (kN) load

Extensometer		Triangular Mesh		Rectangular Mesh	
$\mu\varepsilon_x$	$\mu\varepsilon_y$	$\mu\varepsilon_x$	$\mu\varepsilon_y$	$\mu\varepsilon_x$	$\mu\varepsilon_y$
-10.4	28.3	-9.4	28.3	-7.9	28.3

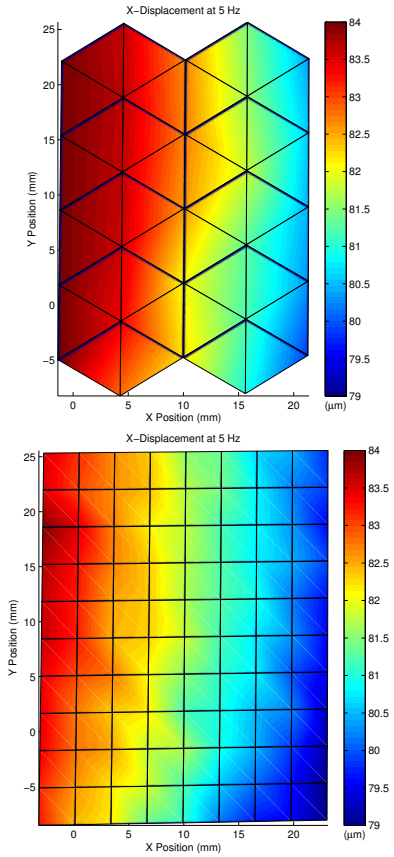

Figure 6. Specimen displacement data in the x-axis.

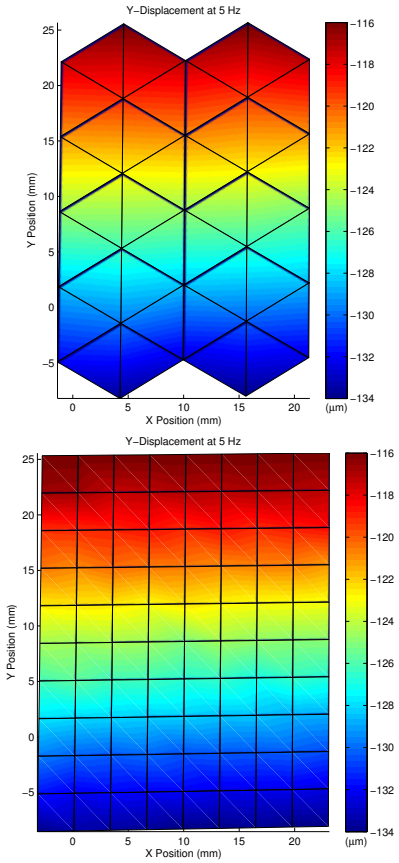

Figure 7. Specimen displacement data in the y-axis.

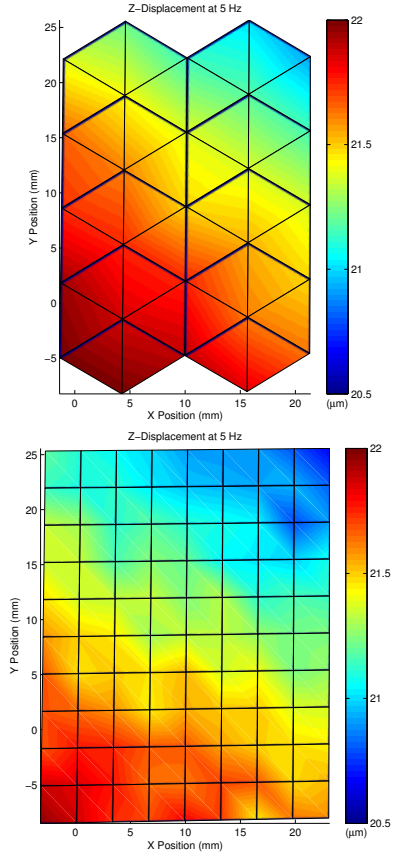

Figure 8. Specimen displacement data in the z-axis.

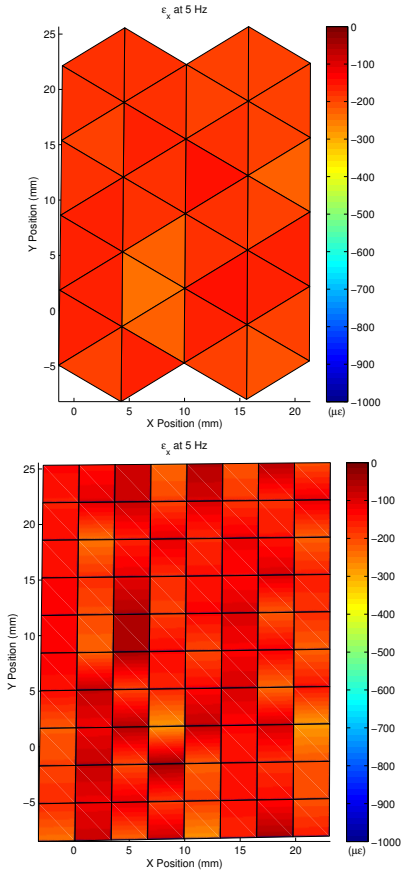

Figure 9. Specimen strain data in the x-axis.

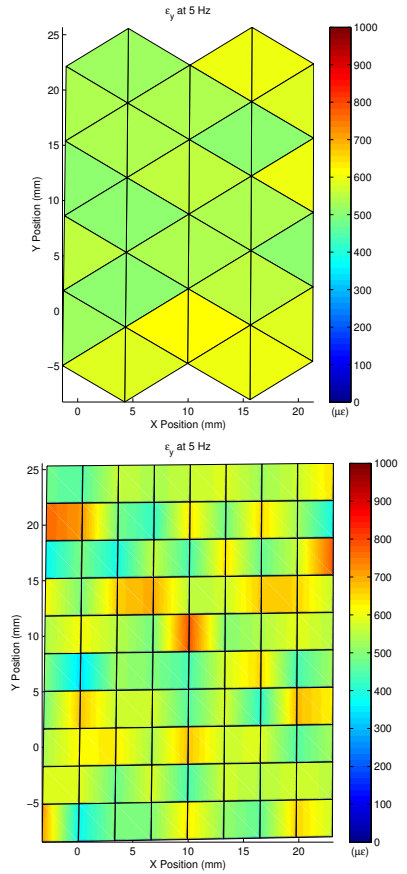

Figure 10. Specimen strain data in the y-axis.

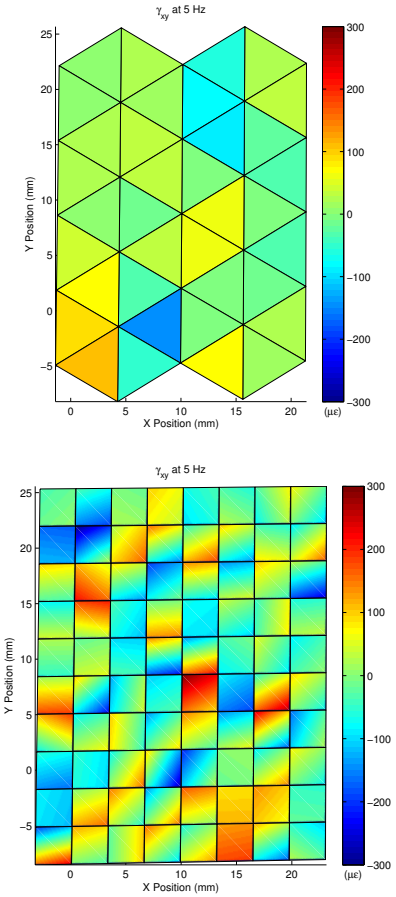

Figure 11. Specimen shear-strain data.

DISCUSSION

When using the laser to measure displacement many of the errors which may occur are insignificant; however, these can corrupt the strain estimates. Discussed below are some of these sources of error, as well as ways in which the common-mode rejection ratio (in this case, the ratio of differential displacement between nodes to their common displacement) can be maximised.

Finite Difference

Like any process employing derivatives, the technique of determining strain from displacement data is sensitive to noise. Noise can take many forms, such as physical disturbances, quantisation noise, spectral leakage and many other sources of error associated with the laser measurement system. These act to perturb the measurements spatially (with displacement errors) and temporally (with phase errors) as illustrated in Figure 12. Therefore, as the element size decreases, the relative magnitude of the errors increases. When the distances between nodes approach the error in displacement, the normalised error in the strain arising from the finite difference may become extremely large. Consequently the fine rectangular grid used in these experiments shows a greater variance of the measured strain when compared with the coarse triangular grid.

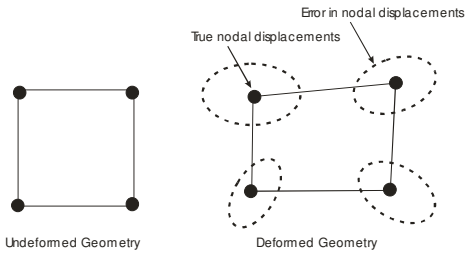

Figure 12. Schematic illustrating how displacement errors affect the strain estimates for small elements.

Quantisation and rigid body motion

Quantisation noise can be minimised by using the full dynamic range of the A/D converters. If there is significant rigid body motion, then the number of bits available for the resolution of the differential motion between nodes is reduced. Hence, the process of estimating strain using the vibrometer is best suited to configurations where there is no or little rigid body motion of the specimen.

In addition, with significant rigid body motion, other sources for uncertainties should also be considered such as alignment, speckle noise, uncertainties in geometry, linearity errors and gain errors.

Alignment of the laser heads

The PSV-3D requires precise alignment of the laser heads. This is a two stage process. Initially a 2D (standard) alignment is conducted for each laser head, which calculates the laser angles for a given point on the live video image. This is followed by a 3D alignment which relates the laser angle to a point in 3D space. For the strain measurements, it is essential that the 3D alignment is extremely accurate.

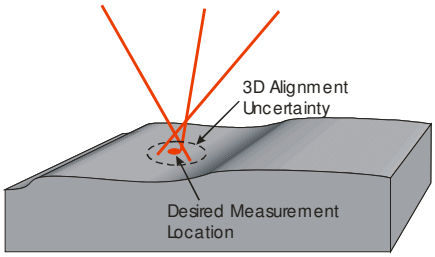

Figure 13. Schematic illustrating result of poor 3D alignment

The quality of the manual 3D alignment of the standard PSV-400-3D is a limitation of the system when dealing with small objects. Without additional measures, the 3D alignment leads to an uncertainty in the beam location of approximately ±2.5mm which effectively means that the three beams do not measure at exactly the same location (as shown in Figure 13). This does not necessarily pose a problem for most applications, especially for large objects, but is a serious problem for strain sensing, to the point of being inadequate for small objects. Polytec have now developed two tools for significantly improving the accuracy for measurements on small objects. The 3D alignment now can be performed on a precise alignment object with accurately measured coordinates instead of using the geometry laser. A software "addition" improves the beam superposition during scans. The PSV-S-TRIA triangulation software optimises the overlap of the three laser beams and corrects the position. It also has the additional benefit that point geometry measurements are improved to an accuracy within approximately 0.1mm. The software requires a high-resolution video camera upgrade.

Alignment of the specimen

To use the planar element shape functions derived above it is important that the specimen is arranged in the x-y plane. This may be simply achieved when defining the coordinate system as part of the 3D alignment.

If there is still some residual misalignment it is possible to correct this once the data is collected. Translation and rotation matrices can be used to "perfectly align" the measurements. Alternatively, shell elements may be used under any reference frame.

Finally, if there is some structural misalignment of the actuators which induces higher order strain motion, such as first order warping modes similar to those found in Zernike Polynomials or Radiation Modes, these can also be removed by spatial convolution. The residual motion (after the contribution from all principal basis functions is removed) should be related to the strain field arising from the applied loads.

Spatial filtering of displacement data

The strain estimates are very sensitive to noise. By spatially filtering the displacement measurements using the appropriate orthogonal basis functions or low pass filters, before applying the Finite Element shape functions, it is possible to improve the estimates of the strains across the surface with some loss of spatial resolution. This technique was commonly employed in early papers measuring bending strain (Xu et al. 1996). A similar technique using FE shape functions has been used to estimate the continuous out-of-plane displacement of a panel using discrete PSV-3D measurements (Halim et al 2008).

Frequency range

Although the specifications for the laser are in mm/s/(sqrt(Hz) (velocity) it is necessary to convert these to displacements in μm/sqrt(Hz) for the exercise of calculating strain. The relationship between velocity v and displacement δ for a sinusoidal response at angular frequency ω is

$$v = \frac{d\delta}{dt} = j\omega\delta = j2\pi f\delta \, .$$

Therefore at a frequency of approximately 0.16Hz there is a one to one relationship between mm/s and mm, so the effective displacement resolution at this frequency is 0.02 μm/sqrt(Hz) for the (VD-07) velocity decoder. For a given velocity, the displacement decreases with increasing frequency. To achieve nanometre displacement accuracy it is necessary to operate above frequencies in the order of 3Hz with a resolution bandwidth of 1Hz. To achieve the same accuracy at lower frequencies it is necessary to reduce the bin width accordingly.

By operating at higher frequencies there is the benefit of reducing the magnitude of uncorrelated noise sources such as ground-borne vibration. The maximum operating frequency of the strain system is bound by the spatial wavelength in the structure. As with any FE based approach, a minimum of three elements are needed per wavelength, preferably six. In addition, the element size should be an order of magnitude bigger than the accuracy of the laser. For example, assuming the three lasers are accurate to within 0.5mm (Figure 13) and that the specimen is undergoing uniaxial strain, then the element size should be 10 times this (5mm), and the wavelength should be greater than 6 times this (30mm). For aluminium and steel (with a longitudinal wave speed of approximately 5000m/s), and, then the upper frequency bound is approximately 150kHz (5000/(0.0005*6*10)).

In practice, the bandwidth of the vibration source or the constraint of operating in the stiffness-controlled region (when trying to measure quasi-static behaviour of specimens) will determine the upper frequency limit.

Signal Processing

Since the strain is obtained via a spatial differential it is very sensitive to noise. Therefore it is important that a high coherence is maintained between the displacement measurements and the reference. If the coherence drops below unity it is important to take sufficient averages to provide a satisfactory confidence interval (Bendat and Piersol 1986).

Coherence can be optimised by using sinusoidal inputs, or by employing the appropriate temporal windows on the data to minimise leakage with broadband signals.

Small strain

It should be noted that the displacement measured in the direction of a laser beam reflects variation at the observation point rather than at a point on the structure. Consequently laser vibrometer measurements are for an Eulerian reference frame, whereas contact strain measurements (such as those provided by strain gauges) are for a Lagrangian reference frame. This imposes restrictions on the types of measurements one may make, and restricts displacements to "small strain" where the Lagrangian derivative approaches the Eulerian derivative. It is for this reason that dynamic tests should be employed where, despite the measured velocities being significant, the displacements are very small and thus Eulerian strain gauge measurements and Lagrangian laser vibrometer measurements are approximately equivalent.

Surface finish issues

The principle of the 3D vibrometer requires the surface to be rough. Each vibrometer must "see" the backscattered light from itself. As each laser must be directed on the surface from a different direction, the measurement is only possible on rough surfaces. Rough surfaces generate speckle effects. Depending on the amplitude of the motion, these effects can generate dropouts in the optical signal, resulting in spikes in the velocity output.

At smaller vibration amplitudes, the probability for dropouts is low, however, the speckle effects can generate small variations in the amplitude of the measured signals. Those amplitude variations can be neglected for normal measurements. When calculating strain as the first derivative of the displacement, those amplitude variations become visible as noise in the strain signal. This noise is automatically reduced by a procedure called "Speckle Tracking" in the scanning vibrometer software. Instead of remaining on the same spot, the lasers perform microscopic movements during the measurement, causing a constant change in the speckle pattern and therefore an averaging out of the corresponding amplitude variations.

Other sources of noise

In many situations, for thin-walled structures the out-of-plane displacements are an order of magnitude larger than the in-plane displacements. This may cause difficulties in trying to measure very small out-of-plane strains since it is likely that external disturbances will act to degrade the measurements.

Ground-borne and air-borne noise may contaminate the measurements. The both of these can be avoided to some extent by isolating the experiment from the noise sources. For example, using a very stiff and highly damped optical breadboard in conjunction with compliant supports can suppress ground-borne vibration, while a quiet environment will minimise the air-borne noise. Similarly, there are certain times of day (after hours) in which ground-borne vibration will be low.

THE FUTURE

The current work has been performed with the standard Polytec PSV-400-3D, which is not ideally adapted for measurements on small objects. Especially for strain calculations, the Lasers must perfectly intersect on the object. Polytec have addressed this issue and is working on means to increase the accuracy for strain measurements. Two options will be released (software for beam superposition with high resolution camera and precise calibration object for 3D alignment). Polytec will also be releasing software to calculate the strain fields in a manner similar to that presented here.

One exciting possibility of the laser-based strain technique is the measurement of three-dimensional strain for plate- and shell-like structures. The PSV-3D allows the measurement of all obscured surfaces via mirrors. Hence it is possible to measure the displacement of both sides of thin structures. In principle, this allows three-dimensional elements to be used to estimate the strain throughout the specimen, not only on the surface as presented here.

An interesting application of this strain measurement technique is for the use in developing strain based damage detection techniques, such as the new technique based on the principle of strain compatibility (Wildy et al. 2008). The PSV-3D would allow validation and optimisation of such techniques without having to resort to large numbers of strain gauges.

CONCLUSIONS

It has been shown that it is possible to use 3D displacement data obtained from a scanning laser vibrometer to estimate the dynamic strain over the surface of a planar structure. The process is very sensitive to systematic errors in the vibrometer measurement system, in particular misalignment errors between heads. A great deal of attention needs to be paid to minimise noise. However, despite the sensitivity of the technique to errors, it shows great promise in providing a new fast non-contact method for accurately measuring the dynamic strain field across the surface of a structure.

ACKNOWLEDGEMENTS

The authors would like to acknowledge the contribution of the reviewers who provided technical and editorial assistance in the preparation of this manuscript.

REFERENCES

Asundi, A. (1996) "Recent advances in photoelastic applications", International conference on fiber optics an photonics, Madras, vol. 3211, 463-473.

Bendat, J.S. and Piersol, A.G. (1986) "Random Data: Analysis and measurement procedures", Wiley.

Colchero, L., Colchero, J., Gómez Herrero, J., Prieto, E., Baró, A. and Huang, W.H. (2002) "Comparison of strain gage and interferometric detection for measurement and control of piezoelectric actuators", *Materials Characterization*, **48**(2-3), 133-140.

Fagan, M.J. (1992), *Finite Element Analysis – Theory and Practice*, Pearson Prentice-Hall.

Gilfrich, J.V. (1998), *Advances in X-Ray Analysis*, Springer, ISBN 0306458039.

Halim, D., Barrault, G. and Cazzolato, B.S. (2008) "Active control experiments on a panel structure using a spatially-weighted objective method with multiple sensors", *Journal of Sound and Vibration*, **315**(1-2), 1-21.

Kardestuncer, K. (1987), *Finite Element Handbook*, McGraw-Hill.

Miles, R.N., Bao, W. and Xu, Y. (1994) "Estimation of random bending strain in a beam from discrete vibration measurements", *Journal of Sound and Vibration*, **174**(2), 191-199.

Mitchell, L.D., West, R.L. and Wicks, A.L. (1998) "An emerging trend in experimental dynamics: Merging of laser-based three-dimensional structural imaging and modal analysis", *Journal of Sound and Vibration*, **211**(3), 323-333.

Moccio, C.A. and Miles, R.N. (1996) "Measurement of the transfer function between bending strain and a transient load using a scanning laser vibrometer", *Journal of Sound and Vibration*, **189**(5), 661-669.

Schüssler, M. (2007) "PSV-3D for strain measurements", Vibrometer technology workshop, Loughborough University.

Schell, J. (2003) "Can we measure bumps on rotating parts?", Polytec Internal Presentation.

Wang, J., Chen, J. and Li, M. (2004) "A URI 4-node quadrilateral element by assumed strain method for nonlinear problems", *Acta Mechanica Sinica*, **20**(6), p10.

Wildy, S.J., Kotousov, A.G. and Codrington, J.D. (2008) "A new passive defect detection technique based on the principle of strain compatibility" *Smart Materials and Structures*, **17**(4).

Xu, Y. and Miles, R.N. (1996) "Full-field random bending strain measurement of a plate from vibration measurements", *Journals of Sound and Vibration*, **191**(5), 847-858.